



## On the Buckling, Post-Buckling and Strength Behavior of Thin-Walled Unequal-Leg Angle Columns

Pedro B. Dinis<sup>1</sup>, Dinar Camotim<sup>1</sup>, Kostas Belivanis<sup>2</sup>, Colter Roskos<sup>2</sup>, Todd Helwig<sup>2</sup>

### Abstract

This paper reports the available results of an ongoing experimental and numerical investigation on the buckling, post-buckling and strength behavior of short-to-intermediate length unequal-leg angle columns. The experimental results, obtained from tests carried out at University of Texas at Austin, consist of initial imperfection measurements, equilibrium paths, failure loads and collapse modes. As for the numerical simulations, they are carried in the code ABAQUS adopting column discretizations into fine meshes of shell and 3D solid finite elements. After presenting and discussing a comparison between the test results and the numerical simulation values, the whole set of results provides the means to shed new light on the controversy raised by Ojalvo (2011), who proposed a continuum model that departs from Wagner's classical hypothesis and leads to higher flexural-torsional buckling loads for unequal-leg angle (asymmetric) columns. Next, a limited parametric study is carried out, in order to obtain a numerical failure load data bank. Finally, the available numerical (mostly) and experimental failure loads are used as the starting point for a few preliminary considerations on the design of thin-walled unequal-leg angle columns, against global failures, by means of the currently codified Direct Strength Method (DSM) strength curve.

### 1. Introduction

The buckling, post-buckling, strength and design of thin-walled equal-leg angle (singly symmetric) columns has attracted the attention of several researchers in the past, namely Kitipornchai & Chan (1987), Adluri & Madugula (1996), Popovic *et al.* (1999), Young (2004), Rasmussen (2005, 2006) and, more recently, Dinis *et al.* (2010, 2012), Shi *et al.* (2011), Mesacasa Jr. (2012), Silvestre *et al.* (2013), Shifferaw & Schafer (2014), Mesacasa Jr. *et al.* (2014), Justiniano (2014) and Dinis & Camotim (2015). As far as the design is concerned, some of these publications devoted a fair amount of work to develop rules and procedures aimed at predicting the ultimate strength of short-to-intermediate (length) columns, adopting mostly local buckling concepts. However, the numerical simulations recently carried out by Dinis *et al.* (2012, 2013, 2015), concerning pin-ended and fixed-ended short-to-intermediate angle columns (i) shed some new light on key mechanical aspects related with the structural response of such members, namely the fact that it is strongly influenced by the length-dependent interaction between

---

<sup>1</sup> ICIST, CERis, DECivil, Instituto Superior Técnico, Universidade de Lisboa, Portugal <dinis@civil.ist.utl.pt>, <dcamotim@civil.ist.utl.pt>

<sup>2</sup> University of Texas at Austin, Austin, TX, USA <kbelivanis@gmail.com>, <colter.roskos@gmail.com>, <thelwig@mail.utexas.edu>

two global buckling modes (major-axis flexural-torsional and minor-axis flexural), and (ii) showed that it is possible to have a single rational approach, based on the Direct Strength Method (DSM), that can handle adequately both pin-ended and fixed-ended equal-leg angle columns.

To the authors' best knowledge, no similar investigation has been conducted for thin-walled unequal-leg angle columns (even if there are some experimental data available concerning aluminum columns under concentric compression and steel columns under eccentric compression – *e.g.*, Liao 1982, Wu 1982 or Liu & Chantel 2011). Therefore, the present work aims at providing a first contribution towards filling this gap. Moreover, since unequal-leg angle columns were the vehicle selected by Ojalvo (2011) to propose a continuum model that departs from Wagner's classical hypothesis and leads to quite higher flexural-torsional buckling loads, the experimental and numerical results obtained from the work presented in this paper are also used to clarify the controversy between Ojalvo's continuum model and Wagner's classical hypothesis.

The paper begins by presenting and discussing a brief comparative study of the buckling behaviors of equal-leg and unequal-leg angle columns, carried out by resorting to Generalized Beam Theory (GBT) analyses and making it possible to characterize the buckling behavior of the columns that are subsequently analyzed experimentally and/or numerically. The available test results of an ongoing experimental investigation that is being carried out at the University of Texas at Austin are then reported, which consist of initial imperfection measurements, equilibrium paths, failure loads and collapse modes concerning four tested specimens (same cross-section dimensions and different intermediate lengths). Then, these experimental results are compared with ABAQUS (Simulia 2008) numerical simulations, carried out with both 3D solid and shell finite elements models. On the basis of the whole set of experimental and numerical results, it is then possible to shed new light on the controversy raised by Ojalvo (2011) that was described in the previous paragraph. Next, a limited parametric study is carried out with the objective of gathering a numerical failure load data bank that, together with the available experimental values, are subsequently used to carry out a preliminary assessment of whether the currently codified DSM global design curve is able to predict adequately global failures of thin-walled unequal-leg angle columns.

## 2. Buckling Behavior

The curves shown in Fig. 1(a) concern fixed-ended angle columns with three different cross-section dimensions, namely  $B_L=5$  in (127 mm),  $B_S=5; 3; 1$  in (127, 76, 25.4 mm) and  $t=1/4$  in (6.35 mm) –  $B_L$  and  $B_S$  are the long and short leg widths, and  $t$  the wall thickness. Each curve (i) provides the variation, with the length  $L$  (logarithmic scale), of the column critical load  $P_{cr}$ , and (ii) was obtained by means of a sequence of GBT buckling analyses performed with the code GBTUL (Bebiano *et al.* 2008a,b) and including 7 deformation modes: 4 global (**1-4**) and 3 local (**5-7**). As for Figs. 1(b<sub>1</sub>)-(b<sub>3</sub>), they display the corresponding GBT-based modal participation diagrams associated with each  $P_{cr}$  vs.  $L$  curve, which provide the GBT deformation mode contributions to the column buckling modes. Finally, Fig. 1(c) shows the buckled mid-height cross-sections obtained for the L5×3×1/4 columns with  $L=50; 100; 200; 600$  in (127; 257; 508; 1524 cm), as well as the in-plane shapes of deformation modes **2-6** (axial extension not shown). These buckling results prompt the following remarks:

- (i) In the equal-leg (L5×5) angle columns, (i<sub>1</sub>)  $P_{cr}$  decreases monotonically with  $L$  and corresponds to *single half-wave* buckling, (i<sub>2</sub>) the torsion mode **4** always plays a key role, as its participation in the critical buckling modes is highly dominant (except in the very long columns), and (i<sub>3</sub>) the buckling mode changes from flexural-torsional (**2+4**) to flexural (**3**) *abruptly* (at  $L=218$  in) – all these features can be clearly observed in Fig. 1(b<sub>1</sub>).

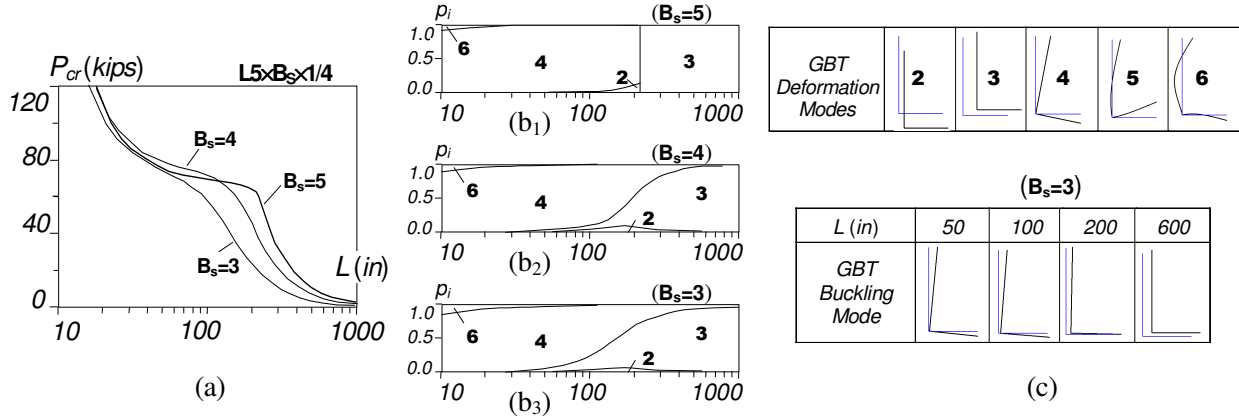


**Figure 1:** (a)  $P_{cr}$  vs.  $L$  curves and (b) GBT modal participation diagrams (columns with  $B_S = 5, 4, 3$  in), and (c) in-plane shapes of first 5 GBT deformations modes and 4 critical buckling modes of columns with  $B_S = 3$  in

- (ii) With exception of the extremely short and long lengths, all unequal-leg angle columns buckle in modes combining torsion (mode 4), minor-axis flexure (mode 3), major-axis flexure (mode 2) and local deformations (mode 6). Torsion is predominant in the shorter lengths and minor-axis flexure in the longer ones, with the transition occurring gradually (major-axis flexure and local deformations always play a minute role) – see Figs. 1(b<sub>2</sub>)-(b<sub>3</sub>). Note that the abrupt buckling mode change mentioned in the previous item ceases to occur in the presence of leg asymmetry.
- (iii) As the leg asymmetry increases ( $L5 \times 4 \rightarrow L5 \times 3$ ), the dominance of the torsion mode 4 decreases slightly in the intermediate length columns, as mode 4 is “replaced” by mode 3 – see Figs. 1(b<sub>2</sub>)-(b<sub>3</sub>).
- (iv) The curve  $P_{cr}(L)$  becomes progressively “smoother” (less slope variation) as the leg asymmetry increases. This is reflected by the gradual disappearance of the curve plateau associated with the intermediate length columns ( $30 < L < 218$  in), which (iv<sub>1</sub>) is clearly visible in the  $L5 \times 5$  column curve, (iv<sub>2</sub>) is barely noticeable in the  $L5 \times 4$  column curve and (iv<sub>3</sub>) vanishes in the  $L5 \times 3$  column curve.

### 2.1 Column Geometry Selection

The angle column geometries (cross-section dimensions and length) were selected in order to ensure that (i) buckling occurs in predominantly torsional modes, (ii) the buckling load is visibly lower than its squash counterpart, calculated for  $f_y = 50$  ksi (344 MPa), thus ensuring the presence of a sizeable elastic post-critical strength. Moreover, since it is planned to test experimentally some of the columns identified, the selection also takes into account the maximum length that can be accommodated by the testing machine: 72 in = 1829 mm. This selection procedure led to the three sets of hot-rolled angle column geometries given in Table 1, together with (i) the associated squash ( $P_y$ ) and critical ( $P_{cr}$ ) loads, with the latter evaluated for  $E = 29000$  ksi (200 GPa) and  $\nu = 0.3$ , (ii) the ratios between them (note that  $P_y$  exceeds  $P_{cr}$  by at least 29%), and (iii) the participations of deformation modes 2-6 in the column critical buckling mode (note that the mode 4 participation dominance and the gradual shift towards mode 3 as  $L$  increases).

## 3. Post-Buckling Behavior and Strength – Experimental Investigation

### 3.1 Test Set-Up and Procedure

This section addresses the experimental investigation, involving unequal-leg angle fixed-ended columns, that was carried out at University of Texas at Austin. A total of four tests have been conducted up to this point: the  $L5 \times 3 \times 1/4$  column set characterized in Table 1 – in order to check the repeatability, two

**Table 1:** Selected column geometries, squash loads, critical buckling loads and modal participations

Cross-section designation	$B_L$ (in)	$B_S$ (in)	$t$ (in)	$A$ (in <sup>2</sup> )	$L$ (in)	$P_y$ (kips)	$P_{cr}$ (kips)	$\frac{P_y}{P_{cr}}$	GBT critical buckling mode deformation mode participation (%)			
									$p_2$	$p_3$	$p_4$	$p_5$
L3×2×3/16	3	2	3/16	0.90	48	73.0	46.0	1.59	1.9	15.8	81.4	0.8
					60		39.9	1.83	2.3	27.0	70.1	0.6
					72		33.1	2.21	2.3	40.1	57.2	0.5
L5×3×1/4	5	3	1/4	1.94	48	97.0	75.3	1.29	0.5	4.5	93.0	1.7
					60		71.3	1.36	0.7	7.1	90.8	1.2
					72		67.7	1.43	1.0	10.5	87.5	0.9
L6×3.5×5/16	6	3.5	5/16	2.87	48	143.5	126.2	1.14	0.4	3.8	93.3	2.2
					60		119.2	1.20	0.6	5.9	91.8	1.6
					72		113.4	1.27	0.8	8.5	89.4	1.2

**Table 2:** Column specimen (i) geometries, (ii) initial geometrical imperfections, (iii) experimental ultimate loads and (iv) observed failure mode nature

Specimen designation	$B_L$ (in.)	$t_L$ (in)	$B_S$ (in)	$t_S$ (in.)	$L$ (in)	$\Delta x$ (in.)	$\Delta z$ (in)	$P_{Exp}$ (kips)	Obs. failure mode nature
L48A	4.985	0.257	3.028	0.255	48 3/16	0.0412	-0.0113	82.3	T
L48B	4.985	0.261	3.021	0.257	48	0.0181	-0.0159	85.8	T
L60	4.980	0.261	3.019	0.258	60 1/16	0.0250	-0.0110	78.8	FT
L72	4.980	0.261	3.023	0.255	72	0.0004	-0.0012	73.1	FT

nearly identical 48 in specimens were tested. The specimens (i) were made of dual grade A36-Grade50 steel and (ii) had the measured cross-section dimensions and lengths given in Table 2.

The tests were conducted in a 550 kip (2447 kN) MTS servo-hydraulic system that was used to apply axial compression to the angle columns – the test set-up, with a specimen installed (prior to testing), is shown in Fig. 2(a). The applied load was measured by means of a 550 kip load cell located in the machine bottom. The tests were performed in displacement-control mode, with an axial displacement rate of 0.05 in (1.27 mm) per minute, in the loading phase, and 0.15 in (3.81 mm) per minute, in the unloading phase. Displacements were measured by means of (i) a built-in displacement meter and (ii) a NDI vision measurement system, which tracked LED markers using six CCD cameras, with an overall accuracy of 0.0004 in (0.01 mm). Four LED markers were placed at sections located (i) one inch from each specimen end and (ii) one foot along the length of the specimen. The LED sensors provided a measure of the initial imperfection of the angle columns prior to testing and, during the tests, the translational displacement measurements provided valuable information about the specimen response evolution – e.g., the translation values were used to determine the specimen torsional rotation at each instrumented location.

In order to achieve fixed-ended support conditions, the angle column end cross-sections were welded to 10×10×1 in (254×254×25.4 mm) plates, which were subsequently bolted to T-shaped end-plates that were gripped in the test set-up as depicted in Fig. 2(b). All bolted and weld connections were aligned with the center of gravity of the unequal leg angle cross-section, in order to ensure pure axial compression.

In order to estimate the specimen initial configuration, four displacements were measured with the help of the LED markers placed along the length and the NDI vision system – Fig. 2(c) shows both the location of the markers (A-D) and the coordinate system adopted. Measurements were taken for an engagement applied load of 0.25 kips and the long and short leg initial imperfections correspond to the variations, along the length of the specimen, of (i) the  $x$ -coordinate between the A and B markers ( $\Delta x$ ) and (ii) the  $z$ -coordinate between the C and D markers ( $\Delta z$ ), respectively. Fig. 2(d) shows the long and

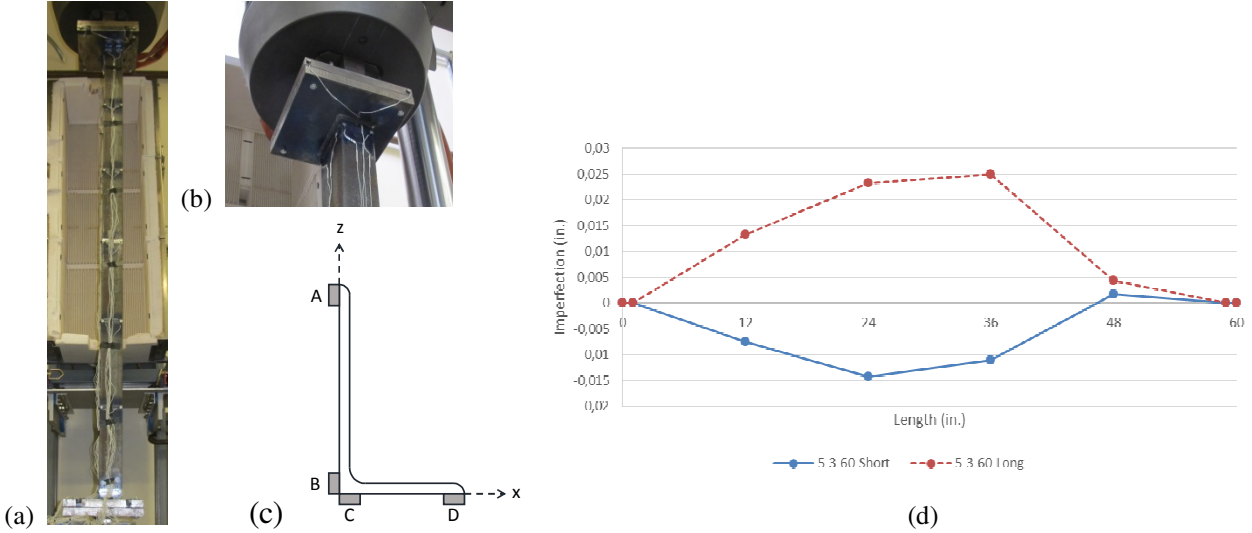


**Figure 2:** (a) Test set-up with specimen installed, (b) end-plate to test set-up connection, (c) cross-section locations of the vision system markers (grey) and (d) initial imperfection profile of the L60 specimen

short leg initial imperfections of the 60in specimen (L60) and Table 2 provides the  $\Delta x$  and  $\Delta z$  values at mid-height for all the specimens tested – in the case of the L60 specimen, these values concern the cross-section nearest to mid-height where measurements were taken (*i.e.*, 36in away from the bottom section).

### 3.2 Test Results

The values of the experimental ultimate loads obtained ( $P_{Exp}$ ) are given in Table 2, which also provides the nature of the observed column failure modes. Two almost identical specimens (L48A and L48B) were tested and the ultimate loads obtained differed by only 4%, thus ensuring test repeatability – the lower ultimate load obtained for the L48A specimen is partly due to the fact that its length is slightly longer than that of the L48B specimen (48 3/16 in vs. 48 in). The tested specimens were observed to fail in two different modes, namely (i) a predominantly torsional mode (labeled “T”), exhibited by the shorter specimens, and (ii) a clear flexural-torsional mode (labeled “FT”), exhibited by the longer specimens – Figs. 3(a)-(b) show the deformed configurations at the brink of collapse of specimens L48A and L60, which clearly evidence the occurrence of torsional and flexural-torsional deformations, respectively.

The observed difference in failure mode nature is in accordance with the buckling results presented and discussed in Section 2. Indeed, the critical buckling mode of the shorter columns contains a higher participation of deformation mode 4 and, consequently, a lower contribution from deformation mode 3 (the sum of the participations of modes 4 and 3 remains practically unaltered) – note the values of  $p_4$  and  $p_3$  in Table 1: 93.0% and 4.5% (L48A specimen), and 90.8% and 7.1% (L60 specimen). It is worth noting that the column failure mode nature is highly sensitive with the respect to the presence of minor-axis flexure (mode 3) in the buckling mode. Indeed, a fairly small  $p_3$  value suffices to entail a FT failure mode similar to the one depicted in Fig. 3(b). In this particular case, the “transition  $p_3$  value” separating columns failing in T and FT modes is comprised between 4.5% and 7.1%.

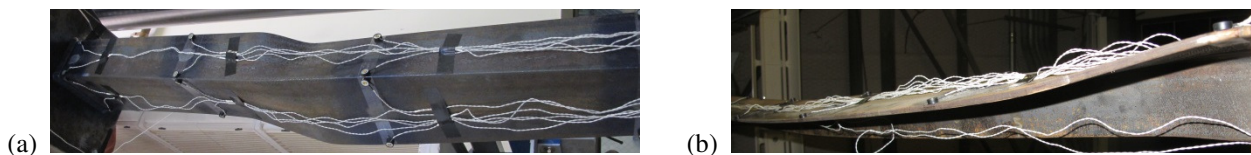


**Figure 3:** Deformed configurations of the (a) L48A and (b) L60 specimens at the onset of collapse

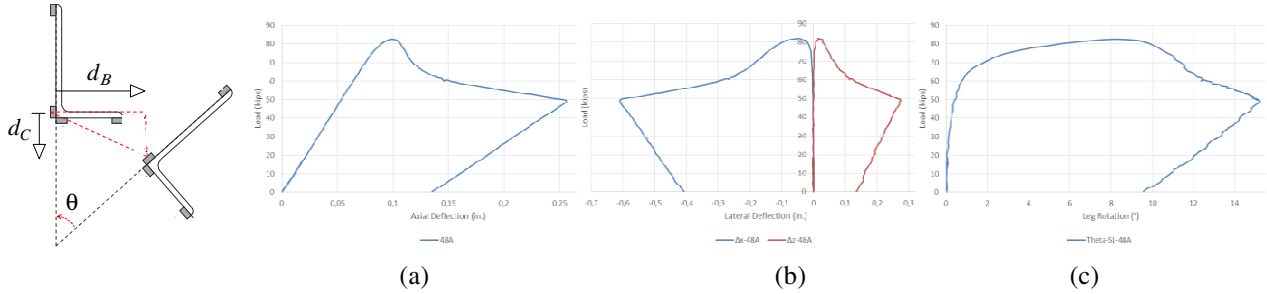


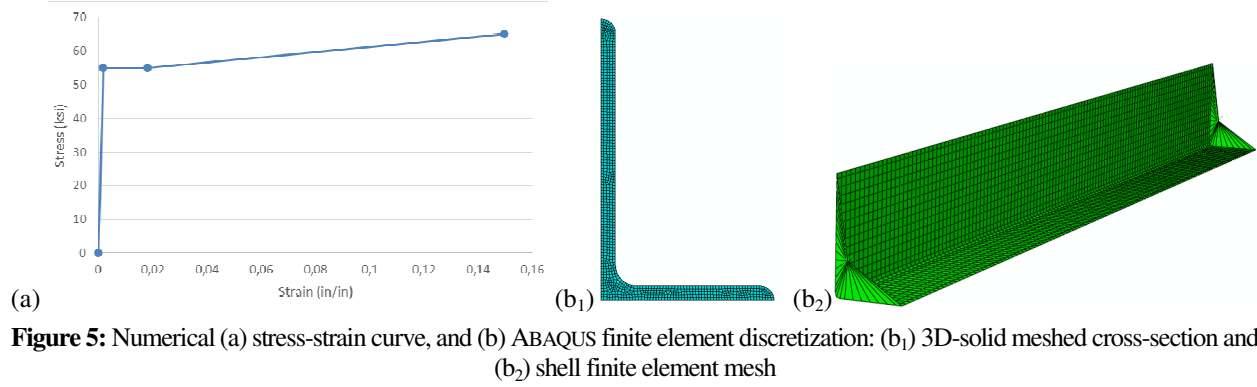
**Figure 4:** Experimental equilibrium paths concerning the L48A specimen: (a)  $P$  vs.  $\epsilon$ , (b)  $P$  vs.  $d_B$  and  $P$  vs.  $d_C$ , and (c)  $P$  vs.  $\theta$

As for Figs. 4(a)-(c), which are intended to illustrate the results obtained from an experimental test, they depict four equilibrium paths concerning specimen L48A, namely (i)  $P$  vs.  $\epsilon$ , where  $\epsilon$  the column axial shortening (Fig. 4(a)), (ii)  $P$  vs.  $d_B$  and  $P$  vs.  $d_C$ , where  $d_B$  and  $d_C$  are the mid-height corner horizontal and vertical displacements (Fig. 4(b)), and (iii)  $P$  vs.  $\theta$  (Fig. 4(c)), where  $\theta$  is the mid-height cross-section torsional rotation – obviously,  $P$  is the applied load. Similar equilibrium paths concerning the other tested specimens are not shown here, although the corresponding information has been recorded – some of them will be shown in Section 4, in the context of the comparison with values yielded by numerical simulations.

#### 4. Post-Buckling Behavior and Strength – Numerical Simulations

This section deals with the numerical simulation of the experimental tests by means of finite element analyses carried out in the code ABAQUS. Before presenting the numerical results obtained and comparing them with the experimental values, it is important to clarify the assumptions adopted while performing the numerical analyses reported herein:

- (i) The dual grade A36-Grade50 steel is deemed homogeneous and isotropic, with an elastic-plastic behavior described by a multi-linear model defined by  $E=30000\text{ksi}$  (207 GPa),  $\nu=0.3$  and  $f_y=55\text{ksi}$  (379 MPa). It approximates the real steel stress-strain curve by linear segments connecting three stress and strain values ( $f=55; 55; 65\text{ksi}$  and  $\epsilon=0.00183; 0.01833; 0.15$ ) – Fig. 5(a) depicts the stress-strain curve adopted in the numerical simulations.
- (ii) The column end sections are fixed: only the axial translation of the loaded end section is possible.
- (iii) Residual stresses (not measured in the tested specimens) are not considered.
- (iv) The initial geometrical imperfections correspond to critical-mode initial imperfection shapes with amplitude equal to the measured long leg imperfection at mid-height ( $\Delta x$  values shown in Table 2) – other possible options will be explored and reported in the near future, namely taking into account the initial imperfection longitudinal profile actually measured in the tested specimens (see Fig. 2(d)).
- (v) The angle columns were analyzed by either 3D-solid or shell finite element analyses. In the former case, the columns were discretized into fine meshes of C3D8R (reduced integration 8-node linear brick) elements that ( $v_1$ ) take into account the nominal hot-rolled cross-section geometry (*i.e.*, rounded corner and leg ends – area  $A=1.94\text{in}^2$  or  $1252\text{mm}^2$ ) and ( $v_2$ ) exhibit an aspect ratio of 4 to 1, with 5 elements through the wall thickness – see Fig. 5(b<sub>1</sub>). The shell finite element model adopted column discretizations into fine S4 (4-node) element meshes (length-to-width ratio below 2) that ( $v_1$ ) also accounted for the rounded corner and leg ends (four rounded corner and one leg end element, respectively with  $t=0.29; 0.344; 0.344; 0.29\text{in}$  and  $t=0.20\text{in}$ , leading to  $A=1.941\text{in}^2$ ), and ( $v_2$ ) modeled the column supports by attaching rigid plates to their end section centroids – see Fig. 5(b<sub>2</sub>).



Figures 6(a)-(b) show a comparison between the numerical and experimental equilibrium paths  $P$  vs.  $\epsilon$ ,  $P$  vs.  $d_B$  and  $P$  vs.  $d_C$  concerning specimens L48B, L60 and L72 – note that (i) the  $N_{solid}$  and  $N_{shell}$  curves correspond to numerical 3D-solid and shell finite element results, respectively, and (ii) the positive displacements are in accordance with the axis orientations shown in Fig. 2(c). As for Fig. 6(c), it displays the experimental and numerical failure modes (deformed configuration close to the peak load) of columns L48B and L72 – the latter, obtained with shell finite elements, include the plastic strain distributions. The analysis of these results prompts the following comments:

- (i) Both the numerical  $N_{solid}$  and  $N_{shell}$  equilibrium paths follow quite closely their experimental counterparts. In particular, note that the numerical (i<sub>1</sub>)  $\epsilon$  curve of specimen L48B and (i<sub>2</sub>)  $d_B$  and  $d_C$  curves of specimen L60 practically coincide with the experimental measurements. Moreover, the numerical ( $P_{Num}$ ) and experimental ( $P_{Exp}$ ) failure loads, given in Table 3, are also quite close: the differences are always below 3.9% (3D-solid) and 3.3% (shell).
- (ii) Nevertheless, there are some differences between the experimental and numerical results, namely in the equilibrium paths (ii<sub>1</sub>) the  $P$  vs.  $\epsilon$  (L60 and L72 specimens) and (ii<sub>2</sub>) the  $P$  vs.  $d_B$  and  $d_C$  (L48B specimen). The authors believe that these discrepancies stem from the joint effect of adopting an approximate initial imperfection shape and neglecting the residual stresses (not measured in the tests).
- (iii) As shown in Fig. 6(c), there is a quite satisfactory match between the ABAQUS shell failure modes and the collapse mechanisms observed during the tests: while the shorter columns collapse in flexural-torsional modes that are predominantly torsional (flexure barely visible and plastic deformations mostly localized at mid-height – see Fig. 6(c<sub>1</sub>)), the longer members fail in flexural-torsional modes that combine visible contributions of flexure and torsion (yielding occurs mostly in the vicinity the supports, particularly in the short leg zone – see Fig. 6(c<sub>2</sub>)).
- (iv) A more thorough numerical investigation is planned for the near future, in order to acquire in-depth knowledge concerning the (iv<sub>1</sub>) column imperfection-sensitivity (taking into account the initial imperfection longitudinal profile, which was measured in the tested specimens) and (iv<sub>2</sub>) the influence of the residual stresses.

**Table 3:** Column specimen experimental and numerical failure loads

Specimen	$P_{Exp}$ (kips)	$P_{Num}$ (kips) – ABAQUS	
		Solid	Shell
L48A	82.31	85.51	82.90
L48B	85.85	85.51	83.00
L60	78.83	80.93	78.51
L72	73.09	75.41	74.56

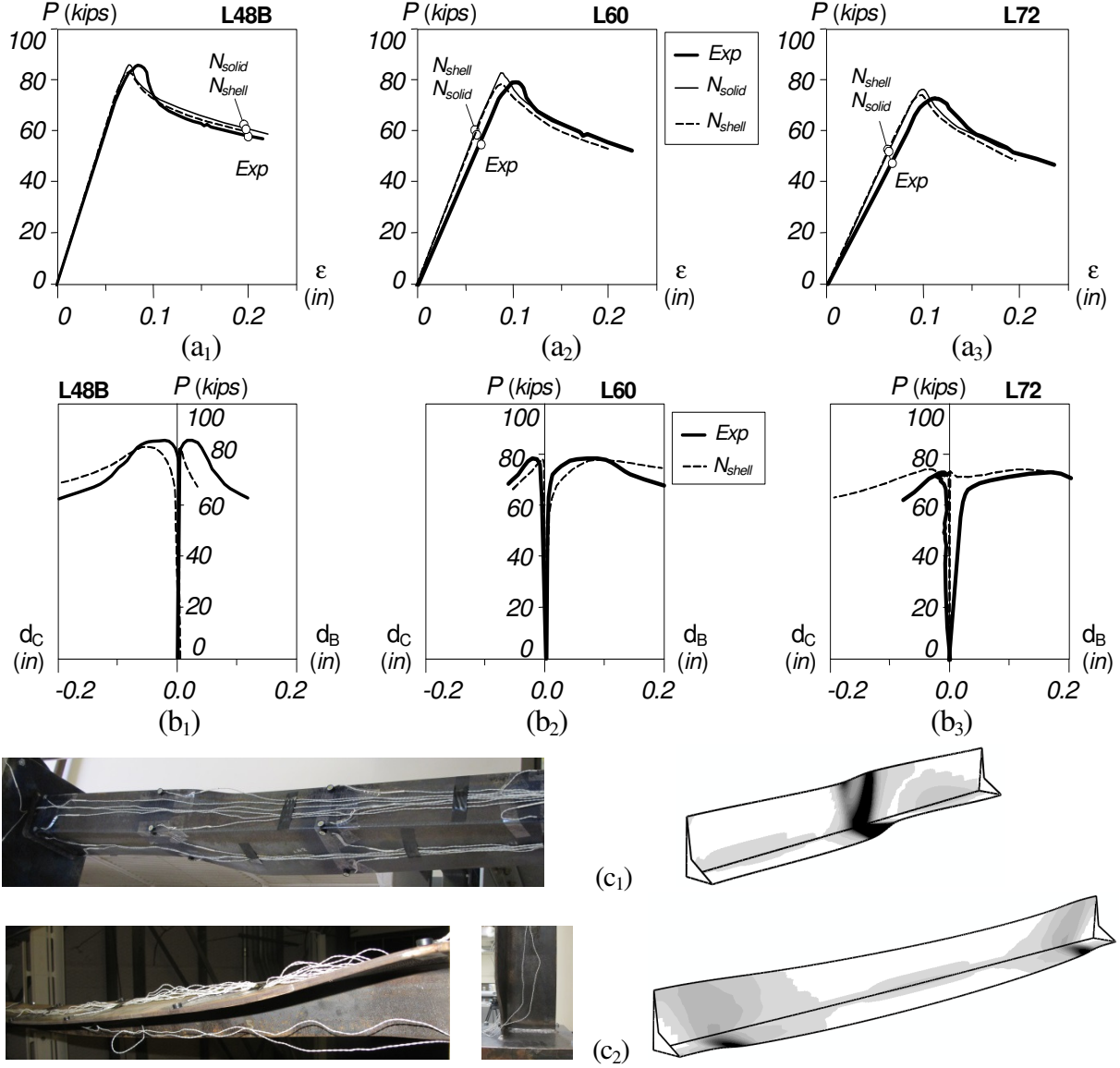


**Figure 6:** Numerical and experimental results concerning specimens L48B, L60 and L72: (a)  $P$  vs.  $\varepsilon$ , (b)  $P$  vs.  $d_B$  and  $P$  vs.  $d_C$  equilibrium paths, and (c) experimental and numerical (shell) failure mode configurations

## 5. Discussion of Ojalvo's Results (2011)

It is well known (*e.g.*, Chages 1974) that the critical global buckling load of asymmetric columns is given by the lowest solution ( $P$  value) of equation

$$-P^3 \left( 1 - \frac{x_0^2}{r^2} - \frac{y_0^2}{r^2} \right) + P^2 \left[ P_x \left( 1 - \frac{y_0^2}{r^2} \right) + P_y \left( 1 - \frac{x_0^2}{r^2} \right) + P_w \right] - P (P_x P_y + P_y P_w + P_x P_w) + P_x P_y P_w = 0 \quad , \quad (1)$$

which was used by Ojalvo (2011) to analyze the fixed-ended unequal-leg angle columns dealt with in this work. In this equation, (i)  $P_x = \pi^2 EI_x / (0.5L)^2$ ,  $P_y = \pi^2 EI_y / (0.5L)^2$ ,  $P_w = (\pi^2 EI_w / (0.5L)^2 + GJ) / r^2$  are the column pure flexural and torsional critical buckling loads, (ii)  $EI_y$  and  $EI_x$  are the major and minor-axis bending stiffness, (iii)  $GJ$  is the Saint-Venant (uniform) torsion stiffness, (iv)  $EI_w$  is the secondary warping

(non-uniform torsion) stiffness, (v)  $x_0$  and  $y_0$  are the shear center coordinates along  $x$  and  $y$  (minor and major principal centroidal axes) and (vi)  $r^2$  is a quantity that is at the root of the discrepancy between the classical theory and the theory proposed by Ojalvo (2011). The former, which is nowadays universally accepted, states that  $r^2$  is the cross-section polar radius of gyration with respect to its shear center divided by the cross-section area  $A$  – adopting Ojalvo’s terminology, this definition stems from a multifilament (or fiber) model – the M model. On the other hand, according to the continuum model proposed by Ojalvo (the C model)  $r^2$  is the square of the distance between the centroid and the shear center. The above discrepancy stems from the different assumptions adopted by the two models concerning the position of the “normal plane” on which the internal bending moments, torsional moment, shear forces and bimoment are defined: either (i) the plane perpendicular to the centroidal axis (C model – Ojalvo’s hypothesis) or (ii) the plane perpendicular to the shear centre axis (M model – Wagner’s hypothesis). Note that the adoption of the C model leads to the vanishing of the cubic term in Eq. (1) – it then becomes quadratic.

Table 4, part of which consists of the experimental and numerical failure loads already reported in Table 3, includes the critical buckling loads of the tested columns (specimens L48, L60 and L72) provided by (i) the ABAQUS 3D solid and shell finite element analyses and (ii) the M and C models, for  $E=30000$ ksi and  $\nu=0.3$ . Note that the  $L5\times3\times1/4$  angle geometrical properties are  $A=1.94$  in<sup>2</sup> (1252 mm<sup>2</sup>),  $I_x=0.853$  in<sup>4</sup> (355045 mm<sup>4</sup>),  $I_y=5.697$  in<sup>4</sup> (2371270 mm<sup>4</sup>),  $I_w=0.0606$  in<sup>6</sup> (16273274 mm<sup>6</sup>),  $J=0.04036$  in<sup>4</sup> (16799 mm<sup>4</sup>),  $x_0=-1.254$  in (-31.854 mm),  $y_0=1.033$  in (-26.231 mm) and  $r^2=2.6392$  in<sup>2</sup> (1703 mm<sup>2</sup>) or  $r^2=6.0154$  in<sup>2</sup> (3881 mm<sup>2</sup>), for the C and M models, respectively.

In order to clarify some behavioral aspects associated with the claim of Ojalvo (2011), some elastic and elastic-plastic shell finite element results are presented in Figs. 7(a)-(c) and 8(a)-(c). They consist of elastic  $P/P_{cr}$  vs.  $\epsilon/\epsilon_{cr}$  equilibrium paths ( $\epsilon_{cr}$  is the column axial shortening for  $P\approx P_{cr}$ ) for columns with lengths  $L=48$  in (Fig. 7(a)),  $L=60$  in (Fig. 7(b)) and  $L=72$  in (Fig. 7(c)) and different end support conditions: end cross-section fully fixed (F), simply supported with warping prevented (SS<sub>WP</sub>) or simply supported with warping free (SS<sub>WF</sub>). As for Figs. 8(a)-(c), they provide the elastic-plastic  $P$  vs.  $\epsilon$  paths for F columns with (i) lengths  $L=48$ ; 60; 72 in ( $P_{cr}=80.2$ ; 75.6; 71.0 kips) and (ii) yield stresses  $f_y=55$ ; 100; 150 ksi ( $P_y=107$ ; 194; 291 kips). The observation of these numerical results prompts the following remarks:

- (i) The  $P_{cr}$  buckling loads obtained through ABAQUS 3D and SFE analysis are quite similar (all differences below 5%, which is perfectly acceptable in view of the assumptions adopted by the shell model) and close to the values provided by the M model (Wagner’s classical hypothesis) – note that the values provided by the M model lie in-between the 3D and SFE numerical results<sup>3</sup>.

**Table 4:** Column specimen experimental and numerical failure loads, numerical critical buckling loads, and squash load

Specimen	$P_{Exp}$ (kips)	ABAQUS				$P_{cr,M}$ (kips)	$P_{cr,C}$ (kips)	$P_y$ (kips)
		$P_{cr}$ (kips)		$P_{Num}$ (kips)				
		Solid	Shell	Solid	Shell			
L48A	82.31	84.03	80.09	85.51	82.90	82.19	148.76	106.70
L48B	85.85	84.03	80.17	85.51	83.00	82.19	148.76	
L60	78.83	79.45	75.60	80.93	78.51	77.19	125.68	
L72	73.09	74.33	71.01	75.41	74.56	72.12	105.53	

<sup>3</sup> At this stage, it is worth noting the differences between the  $P_{cr}$  values appearing in Tables 1 (GBT) and 4 (ABAQUS SFEA), which stem from the fact that the former were obtained by means of buckling analyses that neglected the rounded corners (the cross-section was modeled as the “sum” of two thin rectangles) and, therefore, are lower. Subsequently, the GBT buckling analyses were performed taking into account the rounded corners (approximately) and the  $P_{cr}$  values obtained, which are not shown here, were found to be very close to those given in Table 4 ABAQUS SFEA.

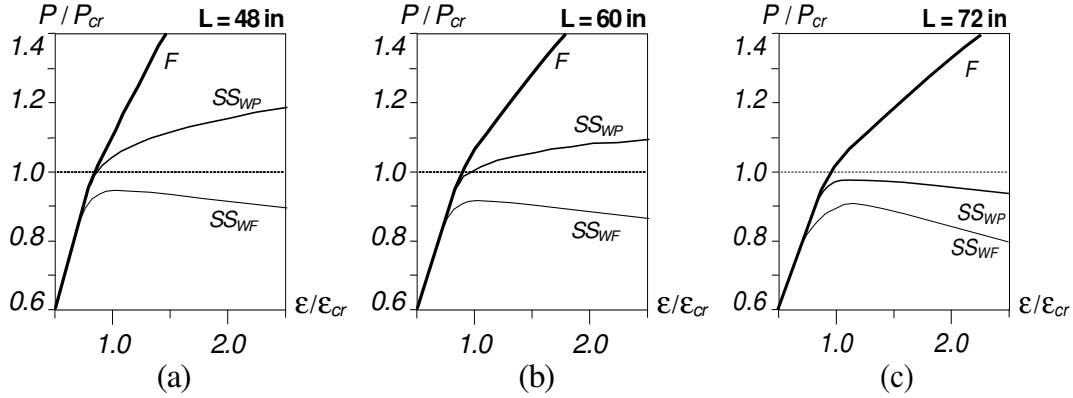


**Figure 7:**  $P/P_{cr}$  vs.  $\epsilon/\epsilon_{cr}$  paths for F,  $SS_{WP}$  and  $SS_{WF}$  columns with lengths (a)  $L=48$  in, (b)  $L=60$  in and (c)  $L=72$  in

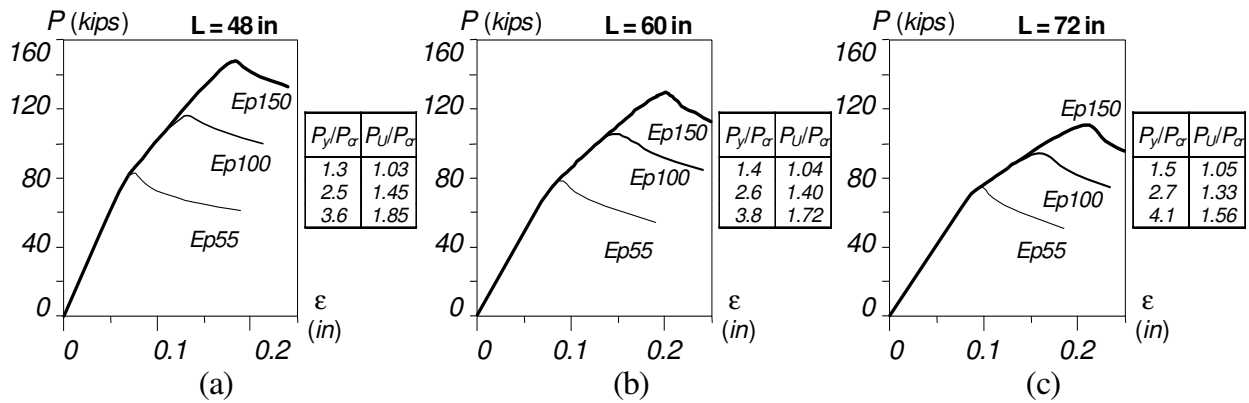


**Figure 8:**  $P$  vs.  $\epsilon$  elastic-plastic equilibrium paths for F columns with (a)  $L=48$  in, (b)  $L=60$  in and (c)  $L=72$  in

- (ii) As already mentioned, the numerical and experimental failure loads compare quite well, as the 3D and SFE values are less than 3.9% and 3.3% apart from the experimental ones.
- (iii) The critical buckling loads provided by the C model exceed significantly the M model ones, thus confirming the results reported by Ojalvo (2011). The differences become more pronounced as the column length decreases: 46% ( $L=72$ ), 63% ( $L=60$ ) and 81% ( $L=48$ ).
- (iv) Ojalvo (2011) argued in support of the higher critical buckling loads obtained with the C model by citing two experimental studies carried out in the Ohio State University (Liao 1982 and Wu 1982) that involved fixed-ended unequal leg ( $L3 \times 2 \times 1/8$  in) aluminum angle columns. The fact that the failure loads obtained are well above the critical buckling loads provided by the M model (and below those provided by the C model) – e.g., a test failure load of 7.62 kips and critical buckling loads of 6.79 (M model) and 8.88 kips (C model) – is used to “support” the validity of the C model, by arguing that “comparisons of failure loads and theoretic buckling loads based on the M model are not what would be expected based on our experience with columns failing in flexural modes, for which the failure load is almost always below the theoretical critical buckling load” (Ojalvo 2011).
- (v) However, the aluminum constitutive law (different from the steel stress-strain curve) and, most of all, the torsional post-critical strength reserve provided by the fixed-ended support conditions amply justify the high (with respect to the critical buckling loads) failure loads obtained experimentally. The equilibrium paths depicted in Figs. 7(a)-(c), concerning  $L=48$ ,  $L=60$  and  $L=72$  columns with F,  $SS_{WP}$  and  $SS_{WF}$  support conditions, illustrate the amount of torsional post-critical strength reserve provided by either fixing the end cross-sections or preventing their warping displacements – note that the

applied load values are normalized with respect to the critical buckling loads provided by the M model. The observation of these equilibrium paths shows that:

- (v.1) Ojalvo’s assertion of “a failure load below the critical buckling load” is only valid for the three  $SS_{WF}$  columns and the longer (L72)  $SS_{WP}$  column.
- (v.2) The three F columns exhibit a fairly large amount of post-critical strength reserve and, except for a very small yield stress, the failure load will certainly exceed the critical buckling load. Figures 8(a)-(c), which display the equilibrium paths of L48, L60 and L72 F columns with three yield stresses ( $f_y=55; 100; 150$  ksi), clearly attest this fact – note that there is a marked influence of the yield stress on the failure loads of the three columns, even if this influence decreases slightly with the length  $L$ .
- (v.3) Since the tests carried out by Liao (1982) and Wu (1982) involved exclusively F columns, it is clear that the corresponding results cannot be used to support the validity of the C model, as stated by Ojalvo (2011) – see item (iv) above.

## 6. DSM Design Considerations

The current DSM strength/design curves for cold-formed steel columns are defined by “Winter-type” expressions that (i) were calibrated against fairly large numbers of experimental and/or numerical results and (ii) provide safe and accurate ultimate strength estimates against local, distortional, global and local-global interactive failures on the sole basis of elastic critical buckling ( $P_{cr,L}$ ,  $P_{cr,D}$ ,  $P_{cr,G}$ ) and squash ( $P_y$ ) loads. In the context of this investigation on unequal-leg angle columns, which are not pre-qualified for the use of the DSM design approach, the relevant nominal strength is  $P_{NG}$  (global, *i.e.*, flexural-torsional) – the currently codified DSM design curves can be found, *e.g.*, in Schafer’s state-of-the-art report (2008).

In order to assess how the global DSM design curve predicts the thin-walled unequal-leg angle columns considered in this work, a limited column failure load data bank is put together next. It comprises (i) the four available test results concerning the experimental investigation under way at University of Texas at Austin (L48A, L48B, L60, L72 specimens) and (ii) numerical values obtained by means of the shell finite element model outlined earlier (see Section 4). The latter concern thin-walled steel ( $E=30000$ ksi,  $\nu=0.3$ ) unequal-leg angle columns exhibiting (i) L3×2×3/16, L5×3×1/4 and L6×3.5×5/16in cross-sections, (ii) lengths equal to 48, 60 and 72 in, and (iii) yield stresses  $f_y=25; 55; 100; 150; 250$  ksi (172; 379; 689; 1034; 1724MPa) – note that, in order to cover a wide critical slenderness  $\lambda_{FT}=(P_y/P_{cr})^{0.5}$  range, several unrealistically high values are considered. All SFE analyses disregard the residual stresses and assume an elastic-perfectly plastic steel constitutive behavior. Moreover, the columns analyzed contain critical-mode initial imperfections with amplitudes equal to the long leg imperfection measured at the specimens L48B, L60, L72 mid-height ( $\Delta x$  values given in Table 2). All the column cross-section dimensions, lengths ( $L$ ), SFEA critical buckling loads ( $P_{cr}$ ), yield stresses and squash loads ( $f_y, P_y$ ), SFEA failure loads ( $P_U$ ) and flexural-torsional slenderness values ( $\lambda_{FT}$ ) are given in Table 5.

Figure 8(a) shows the currently codified global DSM design curve ( $P_{NG}/P_y$  vs.  $\lambda_{FT}$ ) and the experimental (black circles) and numerical (white circles)  $P_U/P_y$  values gathered in this work and concerning fixed-ended unequal-leg angle columns. As for Figs. 8(b<sub>1</sub>)-(b<sub>3</sub>), they plot the numerical  $P_U/P_y$  values against  $\lambda_{FT}$  for each set of 15 columns sharing the same cross-section dimensions (corresponding to all the combinations of the three lengths and five yield stresses given in the previous paragraph), namely the (i) L3×2×3/16 (Fig. 8(b<sub>1</sub>)), (ii) L5×3×1/4 (Fig. 8(b<sub>2</sub>)) and (iii) L6×3.5×5/16 (Fig. 8(b<sub>3</sub>)) columns. The close observation of the results displayed in these figures prompts the following remarks:

**Table 5:** Column numerical and experimental results, including failure load ratios  $P_U/P_y$  (lengths in inches, loads in kips)

Column	$L$	$P_{cr}$	$f_y$	$P_y$	$\lambda_{FT}$	$P_U$	$P_U/P_y$
L3×2×3/16	48	44.2	25	22.5	0.71	21.5	0.96
			55	49.5	1.06	40.4	0.82
			100	90	1.43	47.2	0.52
			150	135	1.75	53.4	0.40
			250	225	2.26	59.3	0.26
L3×2×3/16	60	36.5	25	22.5	0.78	20.9	0.93
			55	49.5	1.16	34.0	0.69
			100	90	1.57	38.0	0.42
			150	135	1.92	41.2	0.31
			250	225	2.48	43.9	0.20
L3×2×3/16	72	29.1	25	22.5	0.88	21.8	0.97
			55	49.5	1.30	29.3	0.59
			100	90	1.76	30.4	0.34
			150	135	2.15	31.9	0.24
			250	225	2.78	33.1	0.15
L5×3×1/4	48	80.2	25	48.5	0.78	48.0	0.99
			55	107	1.15	83.0	0.78
			100	194	1.56	116	0.60
			150	291	1.91	148	0.51
			250	485	2.46	184	0.38
L5×3×1/4	60	75.6	25	48.5	0.80	47.6	0.98
			55	107	1.19	78.5	0.74
			100	194	1.60	106	0.55
			150	291	1.96	130	0.45
			250	485	2.53	151	0.31
L5×3×1/4	72	71.0	25	48.5	0.83	48.4	1.00
			55	107	1.23	74.6	0.70
			100	194	1.65	94.4	0.49
			150	291	2.02	111	0.38
			250	485	2.61	121	0.25
L6×3.5×5/16	48	136.4	25	71.8	0.73	72.8	1.01
			55	158	1.08	135	0.86
			100	287	1.45	186	0.65
			150	431	1.78	242	0.56
			250	718	2.29	316	0.44
L6×3.5×5/16	60	128.4	25	71.8	0.75	72.4	1.01
			55	158	1.11	129	0.82
			100	287	1.50	173	0.60
			150	431	1.83	218	0.51
			250	718	2.36	269	0.37
L6×3.5×5/16	72	121.1	25	71.8	0.77	73.2	1.02
			55	158	1.14	125	0.79
			100	287	1.54	158	0.55
			150	431	1.89	193	0.45
			250	718	2.43	228	0.32
L48A	48	80.1			1.15	82.3	0.77
L48B	48	80.2	55	106.7	1.15	85.9	0.80
L60	60	75.6			1.19	78.8	0.74
L72	72	71.0			1.23	73.1	0.69

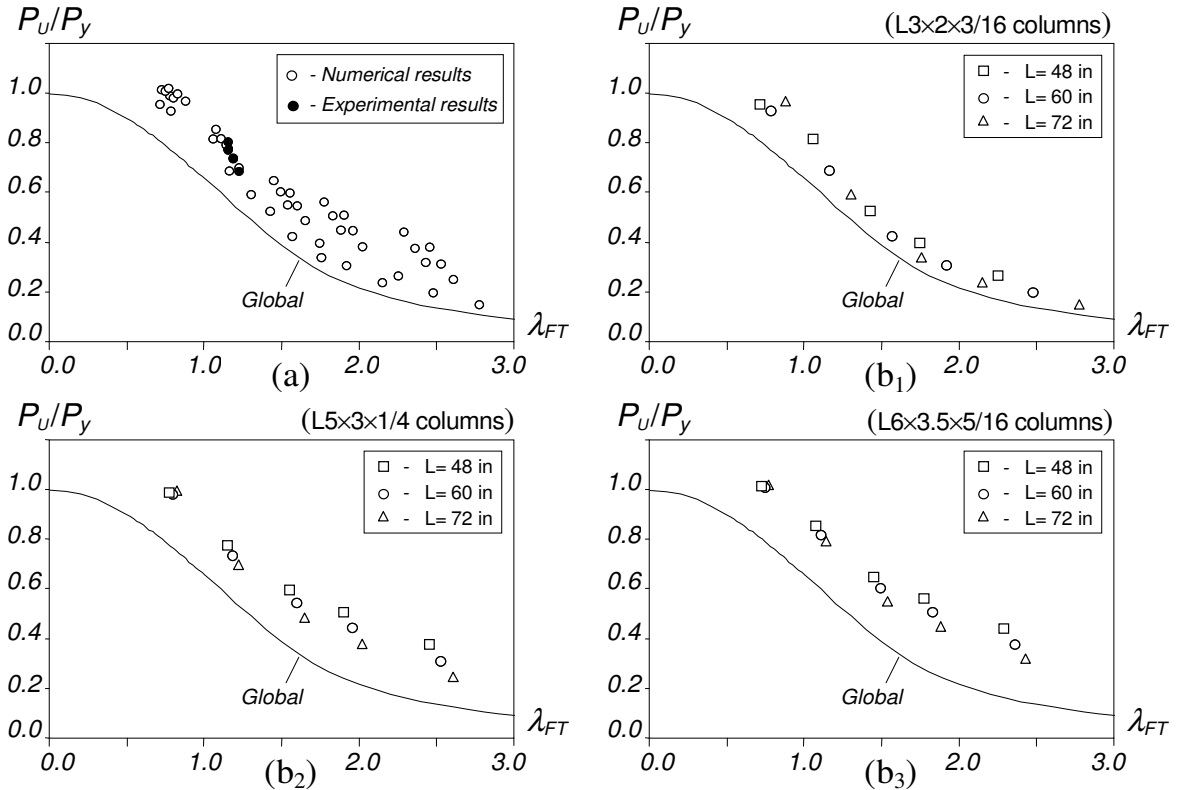


**Figure 8:** Plots  $P_U/P_y$  vs.  $\lambda_{FT}$  for (a) all results and (b) columns (b<sub>1</sub>) L3×32×3/16, (b<sub>1</sub>) L5×3×1/4, (b<sub>3</sub>) L6×3.5×5/16 (numerical)

- (i) First of all, it is worth noticing that, as already mentioned, there is a virtual coincidence between the experimental and numerical  $P_U/P_y$  values concerning the L5×3×1/4 columns with  $f_y=55$  ksi.
- (ii) All  $P_U/P_y$  values lie well above the DSM global design curve, thus meaning that the corresponding predictions are always safe. Nevertheless, it is fair to say that they are too safe, *i.e.*, provide excessive underestimations of the experimental and numerical failure loads. In the authors' opinion, this excessive underestimation stems from the following facts: (ii<sub>1</sub>) the DSM global strength curve was developed mostly on the basis of failure loads from columns collapsing in “predominantly flexural” modes, (ii<sub>2</sub>) the vast majority of the unequal-leg angle columns considered in this work buckle and fail in “predominantly torsional” modes and (ii<sub>3</sub>) fixing the angle column end cross-sections leads to a considerable increase in their torsional post-critical strength reserve, which becomes much larger than the post-critical strength reserve associated with flexural buckling (often taken as synonym of “global buckling”) – this last assertion, readily confirmed by looking at Figs. 7(a)-(c), also applies to thin-walled equal-leg angle and cruciform columns (Dinis & Camotim 2013).
- (iii) Although all the  $P_U/P_y$  values are underestimated by their DSM predictions, the joint observation of Figs. 8(b<sub>1</sub>)-(b<sub>3</sub>) provides a clear indication that such underestimation differs for the (iii<sub>1</sub>) L3×2×3/16 and (iii<sub>2</sub>) L5×3×1/4 + L6×3.5×5/16 columns. Indeed, the predictions concerning the latter columns are visibly safer than those concerning the former, particularly for the higher slenderness values. A closer look at the GBT buckling results corresponding to the three sets of columns provides the explanation for this fact: the participation of minor-axis flexure (mode **3**) in the column flexural-torsional critical buckling mode ( $p_3$  values in Table 1) is much larger in the L3×2×3/16 columns than in their L5×3×1/4 + L6×3.5×5/16 counterparts. Note that these values are, for the lengths  $L=48; 60; 72$  in, (iii<sub>1</sub>)  $p_3=15.8; 27.0; 40.1\%$  (L3×2×3/16), (iii<sub>2</sub>)  $p_3=4.5; 7.1; 10.5\%$  (L5×3×1/4) and (iii<sub>3</sub>)  $p_3=3.8; 5.9; 8.5\%$  (L6×3.5×5/16). The larger amount of flexure in the critical buckling mode leads to a smaller post-critical strength reserve and, therefore, explains the most accurate (less safe) DSM predictions of the L3×2×3/16 column failure loads.
- (iv) The L5×3×1/4 + L6×3.5×5/16 column trios sharing the same yield stress have very close slenderness values, which means that the corresponding  $P_U/P_y$  values are “almost vertically aligned” – moreover, within each column trio, such values decrease slightly with the length. These features are again due to the larger amount of torsion exhibited by the critical buckling mode, if one recalls that the column torsional buckling loads are much less length-dependent than their flexural counterparts – see the  $P_{cr}$  values in Table 5 and note the rates of their drops with the column length: as the length increases from 48 to 72 in,  $P_{cr}$  drops by 34% (L3×2×3/16), 11% (L5×3×1/4) and 11% (L6×3.5×5/16).
- (v) The  $P_U/P_y$  values of the stockier columns ( $\lambda_{FT}<1.0 - f_y=25$  ksi) are all “grouped together”, which reflects the fact that (v<sub>1</sub>) the column collapse is mainly governed by plasticity effects and also that (v<sub>2</sub>) the initial imperfection amplitude included in the  $L=72$  in columns was very small (see Table 2).

## 7. Conclusion

The available results of an ongoing experimental and numerical investigation on the buckling, post-buckling and strength behavior of short-to-intermediate length unequal-leg angle columns were reported. The experimental results, obtained from four column tests carried out at University of Texas at Austin, consisted of initial imperfections, equilibrium paths and collapse loads/modes, providing clear evidence of flexural-torsional failures, which were found to (i) be predominantly torsional for the shorter columns and (ii) combine visible contributions from flexure and torsion for the longer columns. As for the numerical simulations, carried in the code ABAQUS, they (i) adopted column discretizations into fine

meshes of 3D solid or shell finite elements and (ii) concerned three tested specimens – the agreement between the numerical and experimental results was found to be fairly very good, thus providing adequate validation for the two finite element models. Nevertheless, it should be mentioned that it is expected that a more thorough numerical investigation, which is planned for the near future, will make it possible to further improve the existing numerical models, namely by (i) allowing for a more realistic simulation of the column initial geometrical imperfections and (ii) taking into account the presence of unavoidable residual stresses associated with the column fabrication procedure.

Next, the above experimental and numerical results provided the means to fulfill the main objective of this research work, which consists of shedding new light on the controversy raised by Ojalvo (2011) about the elastic flexural-torsional buckling behavior of unequal-leg angle (asymmetric) columns. On the basis of the results reported, it is possible to conclude that the critical buckling loads provided by Ojalvo's model exceed significantly the values determined (i) by adopting Wagner's classical model (GBT and ABAQUS SFEA) and (ii) a full three-dimensional model (ABAQUS 3DFEA) – it was also found that the last two sets of critical buckling loads correlate quite well. Moreover, it was shown that fixing the column end cross-sections considerably increases its flexural-torsional post-buckling strength reserve (particularly if the behavior is predominantly torsional), thus providing a mechanically sound explanation for a feature that Ojalvo (2011) claimed/hoped could be used to support the validity of his model.

Finally, a limited parametric study was carried out to obtain a numerical failure load data bank, which, together with the four experimental failure loads reported in this work, was used as the starting point for a few preliminary considerations on the applicability of the currently codified DSM global strength curve to design of thin-walled unequal-leg angle columns failing in flexural-torsional modes. It was found that this strength curve underestimate all the experimental and numerical failure loads, which means that it can be safely used by designers. However, it was also found that the above underestimation is invariably excessive (particularly when the flexural-torsional buckling/failure mode is predominantly torsional), which stems from the fact that (i) the DSM global strength curve was developed on the basis of failure loads from columns collapsing in “predominantly flexural” modes, (ii) the vast majority of the unequal-leg angle columns considered in this work buckle and fail in “predominantly torsional” modes and (iii) fixing the angle column end cross-sections leads to a considerable increase in their torsional post-critical strength reserve, which is much larger than the flexural buckling counterpart. However, further experimental and numerical results are needed in order to confirm/negate these preliminary findings – the authors are currently working on completing the study presented in this paper and, hopefully, fresh results will be reported in the not too distant future.

## References

- Adluri SMR, Madugula MK (1996). Flexural buckling of steel angles: experimental investigation, *Journal of Structural Engineering* (ASCE), **122**(3), 309-317.
- Bebiano R, Silvestre N, Camotim D (2008a). *GBTUL 1.0 $\beta$  – Code for Buckling and Vibration Analysis of Thin-Walled Members*”, freely available at <http://www.civil.ist.utl.pt/gbt>.
- Bebiano R, Silvestre N, Camotim D (2008b). “GBTUL – a code for the buckling analysis of cold-formed steel members”, *Proceedings of 19<sup>th</sup> International Specialty Conference on Recent Research and Developments in Cold-Formed Steel Design and Construction* (St. Louis, 14-15/10), R. LaBoube, W.-W. Yu (eds.), 61-79.
- Chages A (1974). *Principles of Structural Stability Theory*, Prentice-Hall, Englewood Cliffs.
- Disinis PB, Camotim D (2013). Rational DSM design of thin-walled cruciform and angle columns, *Research and Applications in Structural Engineering, Mechanics and Computation* (SEMC-2013 – Cape Town, 2-4/9), A. Zingoni (ed.), Taylor & Francis (London). (full paper in CD-ROM Proceedings – 1119-1124)

- Dinis PB, Camotim D (2015). A novel DSM-based approach for the rational design of fixed-ended and pin-ended short-to-intermediate thin-walled angle columns, *Thin-Walled Structures*, **87**(February), 158-182.
- Dinis PB, Camotim D, Silvestre N (2010). On the local and global buckling behaviour of angle, T-section and cruciform thin-walled members, *Thin-Walled Structures*, **48**(10-11), 786-797.
- Dinis PB, Camotim D, Silvestre N (2012). On the mechanics of angle column instability, *Thin-Walled Structures*, **52**(March), 80-89.
- Dinis PB, Camotim D, Landesmann A (2013). Towards a more rational DSM design approach for angle columns, *USB Key Drive Proceedings of Structural Stability Research Council Annual Stability Conference* (St. Louis –16-20/4), 471-502.
- Kitipornchai S, Chan SL (1987). Nonlinear finite-element analysis of angle and tee beam-columns, *Journal of Structural Engineering* (ASCE), **113**(4), 721-739.
- Justiniano R (2014). *Behaviour and Design of Angle Columns*, M.A.Sc. Thesis (Structural Engineering), IST, University of Lisbon. (Portuguese)
- Liu Y, Chantel S (2011). Experimental study of steel single unequal-leg angles under eccentric compression, *Journal of Constructional Steel Research*, **67**(6), 919-928.
- Liao KY (1982). *Compression Tests of Unequal Leg Angles*, M.A.Sc. Thesis, Ohio State University, USA.
- Mesacasa Jr. E (2012). *Structural Behavior and Design of Cold-Formed Steel Angle Columns*, M.A.Sc. Thesis in Structural Engineering, School of Engineering at São Carlos, University of S. Paulo, Brazil. (Portuguese)
- Mesacasa Jr. E, Dinis PB, Camotim D, Malite M (2014). Mode interaction and imperfection-sensitivity in thin-walled equal-leg angle columns, *Thin-Walled Structures*, **81**(August), 138-149.
- Ojalvo M (2011). Opposing theories and the buckling strength of unequal-leg angle columns, *Journal of Structural Engineering* (ASCE), **137**(10), 1104-1106.
- Popovic D, Hancock GJ, Rasmussen KJR (1999). Axial compression tests of cold-formed angles, *Journal of Structural Engineering* (ASCE), **125**(5), 515-523.
- Rasmussen KJR (2005). Design of angle columns with locally unstable legs, *Journal of Structural Engineering* (ASCE), **131**(10), 1553-1560.
- Rasmussen KJR (2006). Design of slender angle section beam-columns by the direct strength method, *Journal of Structural Engineering* (ASCE), **132**(2), 204-211.
- Schafer BW (2008). Review: the direct strength method of cold-formed steel member design, *Journal of Constructional Steel Research*, **64**(7-8), 766-778.
- Shi G, Liu Z, Chung KF (2009). Numerical study on the local buckling of 420 MPa steel equal leg angle columns under axial compression, *Proceedings of 6<sup>th</sup> International Conference on Advances in Steel Structures* (ICASS'09 – Hong Kong, 16-18/12), S.L. Chan (ed.), 387-394 (vol. I).
- Shifferaw Y, Schafer BW (2014). Cold-formed steel lipped and plain angle columns with fixed ends, *Thin-Walled Structures*, **80**(July), 142-152.
- Simulia Inc. (2008). *Abaqus Standard* (vrs. 6.7-5).
- Silvestre N, Dinis PB, Camotim D (2013). Developments on the design of cold-formed steel angles, *Journal of Structural Engineering* (ASCE), **139**(5), 680-694.
- Wu FH (1982). *Experimental Determination of Buckling Loads for Unequal Leg Angles with Concentric Loads*, M.A.Sc. Thesis, Ohio State University, USA.
- Young B (2004). Tests and design of fixed-ended cold-formed steel plain angle columns, *Journal of Structural Engineering* (ASCE), **130**(12), 1931-1940.